Fast ultrasound-assisted synthesis of highly crystalline MIL-88A particles and their application as ethylene adsorbents

Juan Amaro-Gahete,[1] Rafael Klee,[1] Dolores Esquivel,* José Rafael Ruiz, César Jiménez-Sanchidrián, Francisco José Romero-Salguero.*

*Corresponding authors

[1] Both authors contributed equally to this work.

Departamento de Química Orgánica, Instituto Universitario de Investigación en Química Fina y Nanoquímica IUIQFN, Facultad de Ciencias, Universidad de Córdoba, Campus de Rabanales, Edificio Marie Curie, E-14071 Córdoba, Spain.

*Corresponding authors: D. Esquivel (e-mail: q12esmem@uco.es, tel.: 957211050); F. J. Romero-Salguero (e-mail: qo2rosaf@uco.es, tel.: 957218638)

Abstract

Highly crystalline MIL-88A particles have been successfully synthesized via fast ultrasound-assisted processes. The influence of the sonication generator and synthesis time on the structure, crystallinity, morphology and surface area of the materials were studied in detail. Under this modified ultrasonic method, X-ray diffraction patterns of MIL-88A particles showed highly crystalline structures in contrast to those reported in literature. Significant differences on surface areas and microporosity were appreciated under ultrasound conditions employed. Specific surface areas in the range between 179 - 359 m^2 g^{-1} were obtained. That material synthesized under ultrasound batch conditions during 1 h had the highest surface area and microporous character. Different particle sizes and morphologies were obtained depending on the synthesis procedure. In general, probe sonicators led to smaller particle sizes. Moreover, a comparative study of the ethylene adsorption of the MIL-88A particles and several common MOFs in the ethylene adsorption was investigated. The results suggest that the modified ultrasound-assisted procedure for the synthesis of MIL-88A is effective to obtain highly crystalline particles, which are very efficient to adsorb ethylene molecules.

Keywords:

MOF, MIL-88A particles, ultrasound irradiation, ethylene adsorption

Introduction

Metal Organic Frameworks (MOFs) have been increasingly studied [1,2] due to their feasibility in applications such as gas storage [3] and separation [4], catalysis, and drug delivery [5], among others. These compounds consist in metal ions coordinated to organic ligands. The combination of these two components in a MOF provides limitless opportunities to tailor different materials with a chosen purpose. One of the most used synthetic routes for MOF particles involves the use of solvothermal conditions [6]. Even though this route exhibits a reasonable good performance in the quality of the obtained product, it requires relative long periods of heating and high temperatures. So, it is still challenging to precisely set the conditions -timing, temperature, solvent, modulating agent- during synthesis to keep the structural integrity of the framework.

Ultrasonic syntheses have been scarcely used for the preparation of MOFs [7,8]. This is an interesting method in which ultrasonic waves interact with the liquid solution generating small bubbles that provoke pressure and temperature alterations. This promotes effective collisions between particles and simplifies the reaction mechanism by helping the product crystallization. This route also enables the coordination reaction, improving surface morphology by facilitating the percolation of the reagents solution into the porous structure of the initial formed crystals, thus aiding a faster and more homogeneous crystal growth [9]. Different MOF materials such as UiO-66, HKUST-1, TMU-34 have been synthesized by ultrasound irradiation showing important effects on the morphology and growth process of their particles [10–13]. Recently, the ultrasound-assisted synthesis of DUT-32 and other Zn(II)-based MOFs have been carried out and their application as drug and pollutant adsorbents have been reported [14–17].

Also, structured coordination polymers have been successfully synthesized by sonochemical routes, validating it as a very attractive method for the preparation of particles with diverse shapes, sizes and morphologies [18]. In addition, the ultrasound-assisted synthesis of composites of MOFs, specifically HKUST-1, with activated carbon or molecularly imprinted polymers, useful as adsorbents, have been reported [19,20].

Iron (III) MOFs have been previously studied by different groups and they have shown their innocuous character in human health for drug delivery [21]. Although Fe-MIL-88 serial MOFs have been produced by ultrasonic synthesis, only poorly crystalline and not well-defined morphology products were obtained in their studies [22]. One of these materials is MIL-88A which possesses a 3D flexible framework based on oxocentered trimers of iron (III) octahedra connected by fumarate dianions, creating interconnected pores and cages with open channels running along the *c* axis [23]. This arrangement provides a large specific surface area and a high porosity, making it attractive for many applications such as CO_2 separation and adsorption [24], photocatalysis for the degradation of organic pollutants under visible light irradiation, [25,26] or biomaterials encapsulation [27]. Its structure has also been studied as a precursor in other applications, for instance electrodes for energy storage. Its flexibility promotes the electrode/electrolyte contact, reduces the mechanical stress because of the volume change during cycling and boosts the electronic conductivity thanks to its derived composites [28,29].

MIL-88A framework exhibits a good concentration of coordinatively unsaturated metal cations, which are the primary interaction sites for guest olefin molecules through π-complexation, thus making it attractive for in the adsorption of gases such as ethylene [30]. In this application, many conditions should be considered

for selecting a proper adsorbent. Tunable pores and open metal sites can notably enhance the C_2H_4 uptake capacity [31]. In addition, cheap ligands and metal salts for synthesis would make more attractive from the industrial point of view [32].

Furthermore, fruit ripening is a post-harvest problem due to inherent ethylene production. This gas generates irreversible changes that lead to rapid quality loss and decay if the fruit is not consumed within a short window of time. Lee and coworkers [33] have demonstrated that accelerated ageing and the initiation of ripening can occur following exposure to ethylene concentrations as low as 0.1 $mL\cdot L^{-1}$, or its equivalent to 4.46 $\mu mol\cdot L^{-1}$. Consequently, ethylene capture and elimination in the packaging process are necessary to hold out "Best before" date. Therefore, technologies to slow down the ripening process after its onset are in high demand [34]. A compromise between good gas inhibition and harmless materials is also necessary [35].

In this work, a modified ultrasonic method demonstrated its feasibility to produce well-defined MIL-88A particles with high crystallinities and high surface areas. The reported methodology provides a simple and fast procedure for the synthesis of MIL-88A materials with improved properties and variable morphologies. In addition, their enhanced surface area makes them attractive for their use as gas adsorbents. These materials showed a good performance in ethylene adsorption, which is comparable to other MOFs studied.

Experimental section

MIL-88A samples were prepared by an ultrasonic assisted procedure using an ethanolic solution of sodium hydroxide as modulating agent according to previous

studies reported about this synthesis method [21,22]. This solution was prepared by dissolving the appropriated amount of sodium hydroxide (PanReac) in absolute ethanol (PanReac) to eventually obtain a 0.05 g NaOH/mL with the minimum amount of water. The presence of water leads to a fast nucleation, generating small-sized particles which interfere with proper crystal formation and growth. $FeCl_3 \cdot 6H_2O$ (PanReac) and fumaric acid (PanReac) in equimolar amounts (1:1) were dissolved in a mixture of dimethylformamide (DMF, PanReac) and the ethanolic solution previously prepared with a proportion in volume 4.5:1 obtaining a 0.8:1 NaOH to Fe ratio in the reaction media. Considering the solvation effect, DMF slows the MOF crystallization rate by strongly solvating Fe(III) ions in the organic media.

A first synthesis was carried out by placing the reagents into an ultrasound bath (*B: Ultrasons, JP Selecta, 150 W*) for 2 h (*Fe-fum-B2*). Then, the final precipitate was recovered by centrifugation at 9000 rpm for 10 min, washed in DMF and in ethanol by redispersion twice. Finally, the sample was dried and activated in a vacuum oven at 85 °C overnight. In addition, a reduction in time to 1 h in the ultrasonic bath was tested (*Fe-fum-B1*).

Also, two ultrasonic probes (*PP: pulsed probe, Cole-Parmer 4710 Series; and CP: continuous probe, Branson Sonifier 150*) immersed in the solution for 10 (*Fe-fum-PP10*) and 5 min (*Fe-fum-PP5*) in the case of PP, and 10 min in the case of CP (*Fe-fum-CP10*) were used. The stirring conditions were set at 750 W 20 kHz and pulse duration of 10 s for probe PP, and 20 W 10 kHz in continuous wave mode for probe PC, respectively. Afterward, the precipitates were recovered by centrifugation, washed and dried as previously described.

The crystalline phases were checked by Powder X-Ray Diffraction (XRD) on a BrukerD8 Discover A25 diffractometer using filtered Cu Kα radiation within a 2θ angle

range between 5º and 30º and a scan rate of a 0.01º/s in continuous mode. The unit cell parameters were calculated with TOPAS software. The crystallite size was calculated using the Scherrer equation for which an average of the five maximum intensity peaks for each pattern, i.e. (010), (011), (110), (022) and (103) diffraction planes, were considered. The non-zero contributions to the reflection width were corrected by using an XRD pattern of pure LaB_6 from which the broadening at Full Width at Half Maximum (FWHM) was taken. This value was subtracted from the closest signals to its angle reflection in our patterns and the result was considered as the instrumental width. This instrumental width was used to correct each reflection broadening in order to be used in the Scherrer equation. Scanning Electron Micrographs (*SEM*) were acquired in a JEOL JSM 7800F microscope. Raman spectroscopy was implemented in a Renishaw Raman instrument (*InVia Raman Microscope*) furnished with a Leica microscope using a green laser light excitation source (532 nm). The specific surface areas were determined from the N_2 adsorption–desorption isotherms measured at liquid nitrogen temperature (-196 ºC) with an Autosorb iQ Station2 (*Quantachrome*). The samples were previously outgassed under vacuum at 120 °C overnight. The isoelectric points of the materials were measured on a Zetasizer Nano ZSP coupled to a MPT-2 titrator using NaOH or HCl to adjust the pH.

The ethylene adsorption measurements were performed with a pure C_2H_4 stream at 0 °C with an Autosorb iQ Station2 (*Quantachrome*). All MIL-88A samples and other MOFs synthetized as previously reported in bibliography (A520-BASF [36], MOF-801[37], UiO-66 [10], and HKUST-1 [38]) were previously outgassed under vacuum at 120 °C overnight.

Results and discussion

The X-ray diffraction patterns of the studied samples revealed a set of narrow well-defined reflections, thus clearly improving the previous patterns reported for this type of synthesis (**Figure 1**) [22]. This highly crystalline structure is as referenced by quite similar to those previously reported by solvothermal synthesis as well as to the simulated XRD pattern (Figure S1) and single-crystal X-ray diffraction [39]. This improved crystallinity for ultrasonic synthesis was observed in all samples, but with an important decrease in the reflections intensity for Fe-fum-PP5. The incidence of such diminution in crystallinity can be understood by the cavitational collapse uniqueness. Ultrasounds create bubbles as high energy microreactors, which leads to the rapid formation of small particles. This interaction is different depending on the sonication generator which affects the framework formation. If the particles do not get enough energy to keep the coordination bond, low crystallinity is inducted by a simple array of the molecules around the metallic center. Shorter synthesis time in ultrasonic bath (0.5 h) and continuous probe (5 min) resulted in X-ray diffraction patterns ascribable to amorphous materials.

The obtained reflections could be indexed in the *P-62c* space group of the hexagonal system as there was previously calculated for this family of dicarboxylic iron compounds [23,40]. Cell parameters for these materials are given in **Table 1**. The improvement in ultrasonic synthesis allowed to match the reflections with the refinement data obtained for single crystal XRD [23]. Highly crystalline patterns were obtained for all samples, except for Fe-fum-PP5. In addition, the appearance of reflections ascribable to impurities was not clearly observed evidencing the validity of the ultrasonic method to provide high purity crystalline samples.

It was expected that different sonication conditions led to the formation of regular crystal shapes according to the coordination system of the iron (III). **Figure 2** shows SEM images of the studied samples. These materials displayed particles with a prismatic central portion (body) and pyramidal end portions (tips). Fe-fum-B2 sample showed large micrometric particles (ca. 2.7-5.4 μm long x 1.6-3.2 μm wide) with defined elongated crystals and rough surfaces. A close inspection of that texture evidenced the presence of subnucleation structures over these large particles. A long sonication period seemed to be the main reason for the generation of smaller aggregates over the first formed crystals. Thus, Fe-fum-B1, which stayed a shorter time (1 h) in the ultrasonic bath, exhibited a smaller crystal size (ca. 1.3 μm long x 0.55 μm wide), still at micrometric level but with a higher definition in their shape. The sample Fe-fum-PP10, synthesized in the pulsed probe sonicator for 10 min, showed a similar crystal morphology. Nevertheless, these crystals were highly compacted in aggregates consisting of primary small particles (ca. 500 nm long x 180 nm wide). A shorter sonication time as in Fe-fum-PP5 (5 min) provoked a significant reduction in crystallinity as revealed by XRD and so this material exhibited irregular particles with different shapes and sizes. Fe-fum-CP10 sample also had very demarcated small crystals with a smooth surface (ca. 900 nm long x 250 nm wide). As can be observed, the sonication time and conditions influence the nucleation rate and crystal growth, which crucially determine the particle size and shape [41]**.** In general, the ultrasound-assisted synthesis leads to smaller particle sizes than the conventional methods based on hydrothermal synthesis, where reported sizes are ca. 2.6 μm long x 0.5 μm wide [26]. Not only the particle size of these materials was different, but also their aspect ratios. Thus, the ratio of the length between opposite tips to the body width was 1.7, 2.4, 2.8

and 4.0 for samples Fe-fum-B2, Fe-fum-B1, Fe-fum-PP10 and Fe-fum-CP10, respectively. In addition, the tip-body-tip length ratio was ca. 1:1:1 for Fe-fum-B2 and Fe-fum-B1, whereas it was 1:2:1 for Fe-fum-PP10 and Fe-fum-CP10. The use of ultrasonic probes with short sonication times (10 min) instead of the bath sonicator with long sonication times (1-2 h) gave rise to particles with higher aspect ratios and smaller sizes.

Nitrogen adsorption-desorption isotherms recorded at –196 ºC are shown in **Figure 3**. The curves for Fe-fum-B2, Fe-fum-B1 and Fe-fum-PP10 samples are characteristic of microporous materials. Fe-fum-B2 and Fe-fum-B1, synthesized under US batch conditions, showed S_{BET} values of 317 and 359 $m^2 \cdot g^{-1}$, respectively (**Table 2**). Unlike, Fe-fum-PP10 synthesized with the pulsed probe PP presented a lower surface area (179 $m^2 \cdot g^{-1}$). In these materials, the presence of a slight hysteresis loop between adsorption and desorption branches at relative pressures P/P_0=0.8-1.0 revealed the presence of some mesopores. However, the main contribution in the surface area was microporous type with percentages of 72%, 82% and 72% for Fe-fum-B2, Fe-fum-B1 and Fe-fum-PP10, respectively. For Fe-fum-CP10, the curves of adsorption-desorption were a combination of type-I and -IV isotherms, being the contribution of the mesoporosity higher than in the other samples. The N_2 adsorption-desorption isotherm for Fe-fum-CP10 showed a smooth increase of volume with the relative pressure which suggests a wide pore size distribution spanning from microporous to mesoporous. Sample Fe-fum-PP5 gave also a wide distribution of pores but mainly in the upper mesopore range with total lack of micropores.

Raman spectra of the samples (**Figure 4**) evidenced the presence of the fumarate ligands in the framework. The band at 1650 cm^{-1} was attributed to the symmetric vibration modes of the C=C, meanwhile the band at 3070 cm^{-1} corresponds to the vibration =C-H, both present in fumaric acid [42]. The band at 1575 cm^{-1} is attributed to the amide group, which can be associated to DMF coordination in the structure [43]. Even though the samples were dried under vacuum at 85 ºC to remove the synthesis and washing solvents (DMF and anhydrous ethanol, respectively), the Raman spectra for all the samples still showed a remarkable band below 3000 cm^{-1} which can be attributed to alkyl groups present in the organic solvents employed. These molecules are strongly attached by surface coordination and their presence was also revealed by the thermogravimetric analysis in **Figure 5**.

The thermogravimetric profile in all samples evidenced three losses. The first weight loss (below 100 ºC) was attributed to the ethanol used in washing. The second loss starting at c.a. 150 ºC was associated to the volatilization of DMF molecules. Slight degradation of the fumaric ligand started decomposing at 170 ºC. The final loss at 275 ºC corresponded to the complete decomposition of the ligand. Above 300 ºC, the weight of MIL-88A was practically constant up to 800 °C.

The easy, fast and inexpensive synthesis of MIL-88A materials makes them promising candidates for gas adsorption. The performance of the MIL-88A samples and other MOFs as ethylene adsorbents was studied (**Table 3**). **Figure 6** depicts the adsorption isotherms of C_2H_4 for all samples. As can be observed, each material exhibited a similar profile with a moderate increase in ethylene adsorption along the whole pressure range. The higher ethylene adsorption was obtained for Fe-fum-B1

sample reaching 1.64 mmol·g^{-1} at atmospheric pressure and 273 K. This uptake capacity can be ascribed to its high crystallinity, optimal morphology and high micropore area. Fe-fum-CP10 and Fe-fum-B2 showed a lower ethylene uptake with 1.16 and 0.90 mmol C_2H_4·g^{-1}, respectively. Even though both samples had similar crystallinity, their textural properties and morphology are quite different and seem to be determinant factors in the adsorption process (see **Figure 2** and **Table 2**). Fe-fum-PP10 showed an adsorption value 0.68 mmol C_2H_4 g^{-1} due to its low surface area (ca. 179 m^2 g^{-1}). The lowest value for ethylene adsorption was obtained by Fe-fum-PP5 (0.60 mmol C_2H_4 g^{-1}). Although this material possesses a surface area comparable to Fe-fum-PP10, the absence of microporous leads to a less interaction with ethylene molecules.

Finally, in order to compare the performance of MIL-88A samples in ethylene adsorption with other materials, several well-known MOFs (A520-BASF, MOF-801, UiO-66, and HKUST-1) were chosen for this study. Their textural properties and ethylene uptake are given in **Table 3**. Most of them have not previously been used as ethylene adsorbents. All the materials analyzed have an adequate pore size to encapsulate the ethylene molecule (4.163 Å [44]). All of them have much higher specific surface areas than MIL-88A. As it can be observed, the adsorption capacity was strongly dependent on the structure and properties of each MOF. Thus, HKUST-1 exhibited the highest ethylene uptake, followed by A520-BASF. If the adsorption isotherms were normalized by square meter (**Figure 7**), MIL-88A, specifically Fe-fum-B1, would have the highest specific uptake, with similar values to HKUST-1 and A520-BASF. However, materials MOF-801 and UiO-66 provided much lower values, both materials with Zr as the metal node. The differences in adsorption capacity for ethylene among the different MOFs materials cannot be attributed to surface charge

divergences determined from measurements of the point of zero charge in solution (Table 3 and Figure S2). It is assumed that metal-π interactions are mainly responsible for the adsorption of ethylene in these materials (**Figure 8**). Accordingly, those MOFs that are more effective for ethylene adsorption must have a higher population of open metal sites, i.e. Lewis acid sites.

The stability of these materials as adsorbents of ethylene was checked by carrying out three consecutive adsorption-desorption cycles with samples Fe-fum-B1 and A520-BASF (Figures S3 and S4). Both materials provided practically identical isotherms in every cycle. The adsorption capacities of Fe fumarate were 1.62, 1.79 and 1.80, whereas those for Al fumarate were 3.92, 3.92 and 3.95. Furthermore, XRD analysis of the samples revealed that they remained intact after three ethylene adsorption-desorption cycles (Figure S5). Consequently, these materials can be reused for the adsorption of ethylene.

According to our results, fumarate-based MOFs, such as MIL-88A, are interesting materials for the adsorption of ethylene. In virtue of their biocompatibility and low cost, they can be considered as materials of choice for their application in the packaging of fruits. Nevertheless, further studies would be required to test these materials under real conditions.

Conclusions

A modified ultrasound method to synthesize MIL-88A crystals with high crystallinity and high surface area has being accomplished. X-ray diffraction of MIL-88A particles showed more crystalline structures than those obtained in previous studies. Depending on the ultrasound conditions and reaction times, particles with different morphology, surface area and porosity were obtained. Those materials obtained using ultrasound probes exhibited smaller particles with a higher aspect ratio than those synthesized in an ultrasound bath. Also, those materials synthesized under ultrasound bath conditions, Fe-fum-B2 and Fe-fum-B1, exhibited higher surface areas and higher proportion of micropores. The incorporation of the fumarate linkers in the structure was confirmed by Raman and thermogravimetric analysis. Furthermore, MIL-88A particles showed a good response for ethylene adsorption. More concretely, Fe-fum-B1 possesses a specific ethylene adsorption comparable to other MOFs, even though its ethylene uptake is lower due to its moderate specific surface area. These materials can be reused several times without appreciable loss of adsorption capacity. The good performance in ethylene adsorption makes them promising materials for ethylene capture and elimination in the packaging of fruits.

Acknowledgements

The authors gratefully acknowledge the financial support from Ramon Areces Foundation, Spanish Ministry of Economy and Competitiveness (Project MAT2013-44463-R), Andalusian Regional Government (FQM-346 group) and Feder Funds. Also, the authors thank the scientific support from the Nanochemistry and Fine Chemistry Research Institute (IUIQFN) at the Córdoba University.

References

[1] C. Wang, D. Liu, W. Lin, Metal-organic frameworks as a tunable platform for designing functional molecular materials, J. Am. Chem. Soc. 137 (2013) 13222-13234.

[2] G. Férey, Hybrid porous solids: past, present, future, Chem. Soc. Rev. 37 (2008) 191–214.

[3] J. Sculley, D. Yuan, H.-C. Zhou, The current status of hydrogen storage in metal–organic frameworks—updated, Energy Environ. Sci. 4 (2011) 2721-2735.

[4] Y.-S. Bae, A.M. Spokoyny, O.K. Farha, R.Q. Snurr, J.T. Hupp, C.A. Mirkin, Separation of gas mixtures using Co(ii) carborane-based porous coordination polymers, Chem. Commun. 46 (2010) 3478-3480.

[5] P. Horcajada, C. Serre, M. Vallet-Regí, M. Sebban, F. Taulelle, G. Férey, Metal–Organic Frameworks as Efficient Materials for Drug Delivery, Angew. Chemie Int. Ed. 45 (2006) 5974–5978.

[6] P. Horcajada, C. Serre, D. Grosso, C. Boissière, S. Perruchas, C. Sanchez, G. Férey, Colloidal Route for Preparing Optical Thin Films of Nanoporous Metal-Organic Frameworks, Adv. Mater. 21 (2009) 1931–1935.

[7] L.-G. Qiu, Z.-Q. Li, Y. Wu, W. Wang, T. Xu, X. Jiang, Facile synthesis of nanocrystals of a microporous metal–organic framework by an ultrasonic method and selective sensing of organoamines, Chem. Commun. 0 (2008) 3642-3644.

[8] Z.-Q. Li, L.-G. Qiu, T. Xu, Y. Wu, W. Wang, Z.-Y. Wu, X. Jiang, Ultrasonic synthesis of the microporous metal–organic framework $Cu_3(BTC)_2$ at ambient temperature and pressure: An efficient and environmentally friendly method, Mater. Lett. 63 (2009) 78–80.

[9] R. Klee, M. Wiatrowski, M.J. Aragón, P. Lavela, G.F. Ortiz, R. Alcántara, J.L.

Tirado, Improved Surface Stability of C+M x O y @Na 3 V 2 (PO 4) 3 Prepared by Ultrasonic Method as Cathode for Sodium-Ion Batteries, ACS Appl. Mater. Interfaces. 9 (2017) 1471–1478.

[10] M.J. Katz, Z.J. Brown, Y.J. Colón, P.W. Siu, K.A. Scheidt, R.Q. Snurr, J.T. Hupp, O.K. Farha, A facile synthesis of UiO-66, UiO-67 and their derivatives, Chem. Commun. 49 (2013) 9449-9451.

[11] Y. Han, M. Liu, K. Li, Y. Zuo, Y. Wei, S. Xu, G. Zhang, C. Song, Z. Zhang, X. Guo, Facile synthesis of morphology and size-controlled zirconium metal–organic framework UiO-66: the role of hydrofluoric acid in crystallization, CrystEngComm. 17 (2015) 6434–6440.

[12] M. Schlesinger, S. Schulze, M. Hietschold, M. Mehring, Evaluation of synthetic methods for microporous metal–organic frameworks exemplified by the competitive formation of $[Cu_2(btc)_3(H2O)_3]$ and $[Cu_2(btc)(OH)(H_2O)]$, Microporous Mesoporous Mater. 132 (2010) 121–127.

[13] S.A.A. Razavi, M.Y. Masoomi, A. Morsali, Morphology-dependent sensing performance of dihydro-tetrazine functionalized MOF toward Al(III), Ultrason. Sonochem. 41 (2018) 17–26.

[14] R. Abazari, G. Salehi, A.R. Mahjoub, Ultrasound-assisted preparation of a nanostructured zinc(II) amine pillar metal-organic framework as a potential sorbent for 2,4-dichlorophenol adsorption from aqueous solution, Ultrason. Sonochem. 46 (2018) 59–67.

[15] R. Abazari, A.R. Mahjoub, Ultrasound-assisted synthesis of Zinc(II)-based metal organic framework nanoparticles in the presence of modulator for adsorption enhancement of 2,4-dichlorophenol and amoxicillin, Ultrason. Sonochem. 42 (2018) 577–584.

[16] R. Abazari, A. Reza Mahjoub, A.M.Z. Slawin, C.L. Carpenter-Warren, Morphology- and size-controlled synthesis of a metal-organic framework under ultrasound irradiation: An efficient carrier for pH responsive release of anti-cancer drugs and their applicability for adsorption of amoxicillin from aqueous solution, Ultrason. Sonochem. 42 (2018) 594–608.

[17] R. Abazari, A.R. Mahjoub, S. Molaie, F. Ghaffarifar, E. Ghasemi, A.M.Z. Slawin, C.L. Carpenter-Warren, The effect of different parameters under ultrasound irradiation for synthesis of new nanostructured Fe_3O_4@bio-MOF as an efficient anti-leishmanial in vitro and in vivo conditions, Ultrason. Sonochem. 43 (2018) 248–261.

[18] S.Y. Hao, Y.H. Li, Z.C. Hao, G.H. Cui, Sonochemical synthesis of two nanostructured silver(I) coordination polymers based on semi-rigid bis(benzimidazole) ligands, Ultrason. Sonochem. 39 (2017) 636–644.

[19] F.N. Azad, M. Ghaedi, K. Dashtian, S. Hajati, V. Pezeshkpour, Ultrasonically assisted hydrothermal synthesis of activated carbon–HKUST-1-MOF hybrid for efficient simultaneous ultrasound-assisted removal of ternary organic dyes and antibacterial investigation: Taguchi optimization, Ultrason. Sonochem. 31 (2016) 383–393.

[20] A. Asfaram, M. Ghaedi, K. Dashtian, Ultrasound assisted combined molecularly imprinted polymer for selective extraction of nicotinamide in human urine and milk samples: Spectrophotometric determination and optimization study, Ultrason. Sonochem. 34 (2017) 640–650.

[21] P. Horcajada, T. Chalati, C. Serre, B. Gillet, C. Sebrie, T. Baati, J.F. Eubank, D. Heurtaux, P. Clayette, C. Kreuz, J.-S. Chang, Y.K. Hwang, V. Marsaud, P.-N. Bories, L. Cynober, S. Gil, G. Férey, P. Couvreur, R. Gref, Porous metal–

organic-framework nanoscale carriers as a potential platform for drug delivery and imaging, Nat. Mater. 9 (2010) 172–178.

[22] T. Chalati, P. Horcajada, R. Gref, P. Couvreur, C. Serre, Optimisation of the synthesis of MOF nanoparticles made of flexible porous iron fumarate MIL-88A, J. Mater. Chem. 21 (2011) 2220–2227.

[23] C. Mellot-Draznieks, C. Serre, S. Surblé, N. Audebrand, G. Férey, Very Large Swelling in Hybrid Frameworks: A Combined Computational and Powder Diffraction Study, J. Am. Chem. Soc. 127 (2005) 16273–16278.

[24] S. Wongsakulphasatch, W. Kiatkittipong, J. Saupsor, J. Chaiwiseshphol, P. Piroonlerkgul, V. Parasuk, S. Assabumrungrat, Effect of Fe open metal site in metal-organic frameworks on post-combustion CO 2 capture performance, Greenh. Gases Sci. Technol. 7 (2017) 383–394.

[25] N. Liu, W. Huang, X. Zhang, L. Tang, L. Wang, Y. Wang, M. Wu, Ultrathin graphene oxide encapsulated in uniform MIL-88A(Fe) for enhanced visible light-driven photodegradation of RhB, Appl. Catal. B Environ. 221 (2018) 119–128.

[26] W.-T. Xu, L. Ma, F. Ke, F.-M. Peng, G.-S. Xu, Y.-H. Shen, J.-F. Zhu, L.-G. Qiu, Y.-P. Yuan, Metal–organic frameworks MIL-88A hexagonal microrods as a new photocatalyst for efficient decolorization of methylene blue dye, Dalt. Trans. 43 (2014) 3792–3798.

[27] G.-Y. Jeong, R. Ricco, K. Liang, J. Ludwig, J.-O. Kim, P. Falcaro, D.-P. Kim, Bioactive MIL-88A Framework Hollow Spheres via Interfacial Reaction In-Droplet Microfluidics for Enzyme and Nanoparticle Encapsulation, Chem. Mater. 27 (2015) 7903–7909.

[28] Q. Ma, H. Song, Q. Zhuang, J. Liu, Z. Zhang, C. Mao, H. Peng, G. Li, K. Chen, Iron-nitrogen-carbon species boosting fast conversion kinetics of Fe 1-x S@C

nanorods as high rate anodes for lithium ion batteries, Chem. Eng. J. 338 (2018) 726–733.

[29] Y. Wang, X. Guo, Z. Wang, M. Lü, B. Wu, Y. Wang, C. Yan, A. Yuan, H. Yang, Controlled pyrolysis of MIL-88A to Fe 2 O 3 @C nanocomposites with varied morphologies and phases for advanced lithium storage, J. Mater. Chem. A. 5 (2017) 25562–25573.

[30] B. Li, Y. Zhang, R. Krishna, K. Yao, Y. Han, Z. Wu, D. Ma, Z. Shi, T. Pham, B. Space, J. Liu, P.K. Thallapally, J. Liu, M. Chrzanowski, S. Ma, Introduction of π-Complexation into Porous Aromatic Framework for Highly Selective Adsorption of Ethylene over Ethane, J. Am. Chem. Soc. 136 (2014) 8654–8660.

[31] J. Wang, D. Xie, Z. Zhang, Q. Yang, H. Xing, Y. Yang, Q. Ren, Z. Bao, Efficient adsorption separation of acetylene and ethylene via supported ionic liquid on metal-organic framework, AIChE J. 63 (2017) 2165–2175.

[32] Y. Zhao, J. Wang, Z. Bao, H. Xing, Z. Zhang, B. Su, Q. Yang, Y. Yang, Q. Ren, Adsorption separation of acetylene and ethylene in a highly thermostable microporous metal-organic framework, Sep. Purif. Technol. 195 (2018) 238–243.

[33] L. Lee, J. Arul, R. Lencki, F. Castaigne, A review on modified atmosphere packaging and preservation of fresh fruits and vegetables: Physiological basis and practical aspects—Part I, Packag. Technol. Sci. 8 (1995) 315–331.

[34] B. Zhang, Y. Luo, K. Kanyuck, G. Bauchan, J. Mowery, P. Zavalij, Development of Metal–Organic Framework for Gaseous Plant Hormone Encapsulation To Manage Ripening of Climacteric Produce, J. Agric. Food Chem. 64 (2016) 5164–5170.

[35] A. Altan, Z. Aytac, T. Uyar, Carvacrol loaded electrospun fibrous films from zein and poly(lactic acid) for active food packaging, Food Hydrocoll. 81 (2018)

48–59.

[36] E. Alvarez, N. Guillou, C. Martineau, B. Bueken, B. Van de Voorde, C. Le Guillouzer, P. Fabry, F. Nouar, F. Taulelle, D. de Vos, J.-S. Chang, K.H. Cho, N. Ramsahye, T. Devic, M. Daturi, G. Maurin, C. Serre, The Structure of the Aluminum Fumarate Metal-Organic Framework A520, Angew. Chemie Int. Ed. 54 (2015) 3664–3668.

[37] H. Furukawa, F. Gándara, Y.-B. Zhang, J. Jiang, W.L. Queen, M.R. Hudson, O.M. Yaghi, Water Adsorption in Porous Metal–Organic Frameworks and Related Materials, J. Am. Chem. Soc. 136 (2014) 4369–4381.

[38] K.-S. Lin, A.K. Adhikari, C.-N. Ku, C.-L. Chiang, H. Kuo, Synthesis and characterization of porous HKUST-1 metal organic frameworks for hydrogen storage, Int. J. Hydrogen Energy. 37 (2012) 13865–13871.

[39] C. Serre, F. Millange, S. Surblé, G. Férey, A Route to the Synthesis of Trivalent Transition-Metal Porous Carboxylates with Trimeric Secondary Building Units, Angew. Chemie Int. Ed. 43 (2004) 6285–6289.

[40] C. Serre, C. Mellot-Draznieks, S. Surble, N. Audebrand, Y. Filinchuk, G. Ferey, Role of Solvent-Host Interactions That Lead to Very Large Swelling of Hybrid Frameworks, Science 315 (2007) 1828–1831.

[41] N.L. Torad, M. Hu, Y. Kamachi, K. Takai, M. Imura, M. Naito, Y. Yamauchi, Facile synthesis of nanoporous carbons with controlled particle sizes by direct carbonization of monodispersed ZIF-8 crystals, Chem. Commun. 49 (2013) 2521-2523.

[42] J. Wang, J. Wan, Y. Ma, Y. Wang, M. Pu, Z. Guan, Metal–organic frameworks MIL-88A with suitable synthesis conditions and optimal dosage for effective catalytic degradation of Orange G through persulfate activation, RSC Adv. 6

(2016) 112502–112511.

[43] E.Y. Ionashiro, F.J. Caires, A.B. Siqueira, L.S. Lima, C.T. Carvalho, Thermal behaviour of fumaric acid, sodium fumarate and its compounds with light trivalent lanthanides in air atmosphere, J. Therm. Anal. Calorim. 108 (2012) 1183–1188.

[44] S. Sircar, A.L. Myers, Gas Separation by Zeolites. In Handbook of Zeolite Science and Technology; S.M Anesbach, K.A. Carrado, P.K. Dutta, Eds.; Marcel Dekker Inc. New York, 2003.

[45] G. Maurin, Role of molecular simulations in the structure exploration of Metal-Organic Frameworks: Illustrations through recent advances in the field, Comptes Rendus Chim. 19 (2016) 207–215.

[46] K. Trepte, J. Schaber, S. Schwalbe, F. Drache, I. Senkovska, S. Kaskel, J. Kortus, E. Brunner, G. Seifert, The origin of the measured chemical shift of 129 Xe in UiO-66 and UiO-67 revealed by DFT investigations, Phys. Chem. Chem. Phys. 19 (2017) 10020–10027.

Table 1. Unit cell parameters in the space group *P-62c* of the hexagonal system for the synthesized MIL-88A samples.

	Fe-fum-B2	Fe-fum-B1	Fe-fum-PP10	Fe-fum-PP5	Fe-fum-CP10
a / Å	13.349 (2)	13.449 (1)	13.350 (1)	13.298 (1)	13.159 (2)
c / Å	12.515 (6)	12.553 (3)	12.506 (5)	12.420 (1)	12.300 (4)
Volume / $Å^3$	1931.3 (2)	1966.2 (6)	1930.2 (4)	1899.7 (8)	1844.5 (1)
Crystallite size (nm)	88.7	77.2	72.2	55.2	67.2

Table 2. BET Surface, External area, Micropore area, Micropore volume, Pore volume and width (DFT) calculated from the N_2 adsorption isotherms for the MIL88A samples.

Sample	**S_{BET} ($m^2 \cdot g^{-1}$)**	**External area ($m^2 \cdot g^{-1}$)**	**Micropore area V-t method ($m^2 \cdot g^{-1}$)**	**Micropore volume V-t method ($cm^3 \cdot g^{-1}$)**	**Pore volume DFT ($cm^3 \cdot g^{-1}$)**
Fe-fum-B2	317	88	229	0.092	0.256
Fe-fum-B1	359	63	296	0.118	0.179
Fe-fum-PP10	179	50	129	0.052	0.162
Fe-fum-PP5	189	189	-	-	0.306
Fe-fum-CP10	352	162	189	0.080	0.253

Table 3. S_{BET} of studied MOF materials and their ethylene adsorption performance.

Material	**Metallic center**	**Organic linker**	**S_{BET} ($m^2\ g^{-1}$)**	**Pore size (Å)** (*reported in literature*)	**Point of zero charge values**	**Ethylene adsorption ($mmol \cdot g^{-1}$)**
Fe-fum-B1	Fe	Fumaric acid	359	6.0 [21]	6.6	1.63
A520-BASF	Al	Fumaric acid	911	5.8 [45]	6.9	3.90
MOF-801	Zr	Fumaric acid	856	4.8, 5.6, 7.4 [37]	4.3	2.31
UiO-66	Zr	1,4-benzenedicarboxylic acid	1400	7.5, 12 [46]	6.0	2.61
HKUST-1	Cu	1,3,5-benzenetricarboxylic acid	2042	9 [38]	3.3	8.33

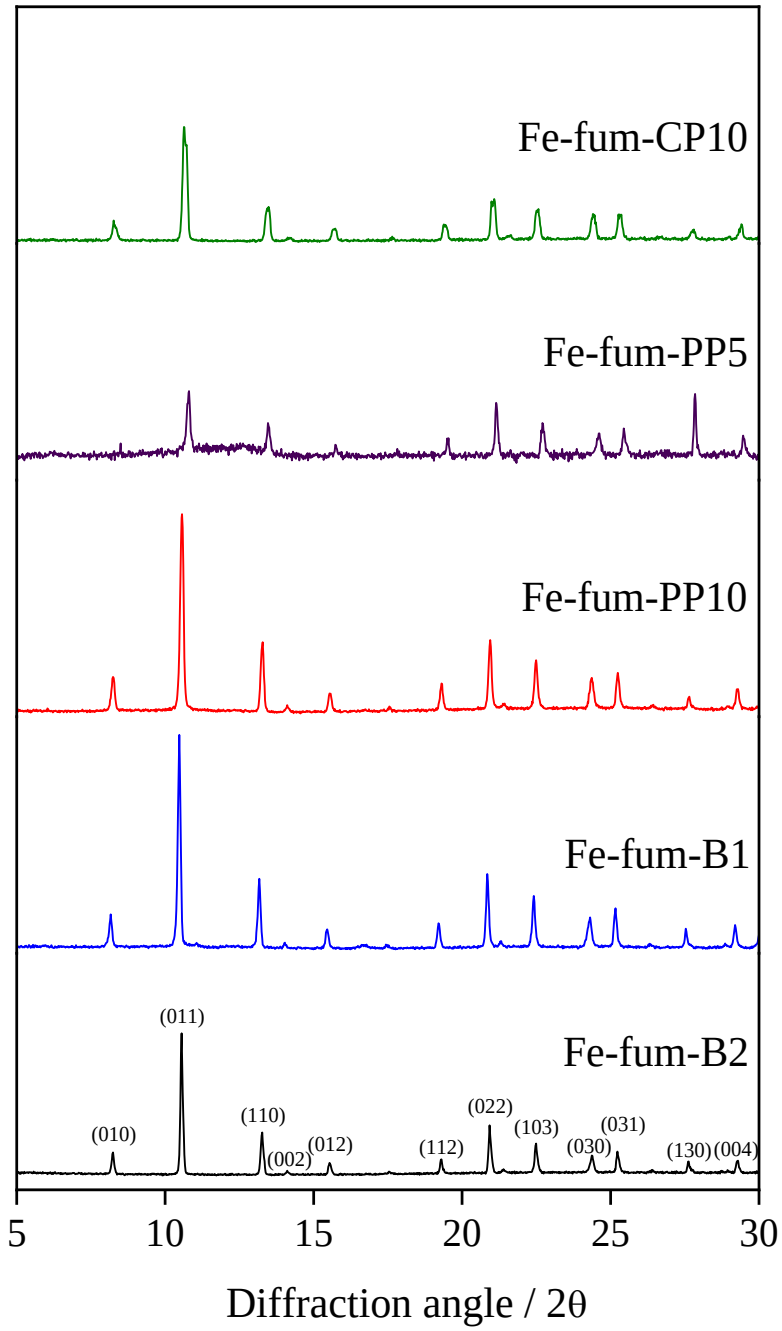

Figure 1. X Ray Diffraction patterns of MIL-88A samples.

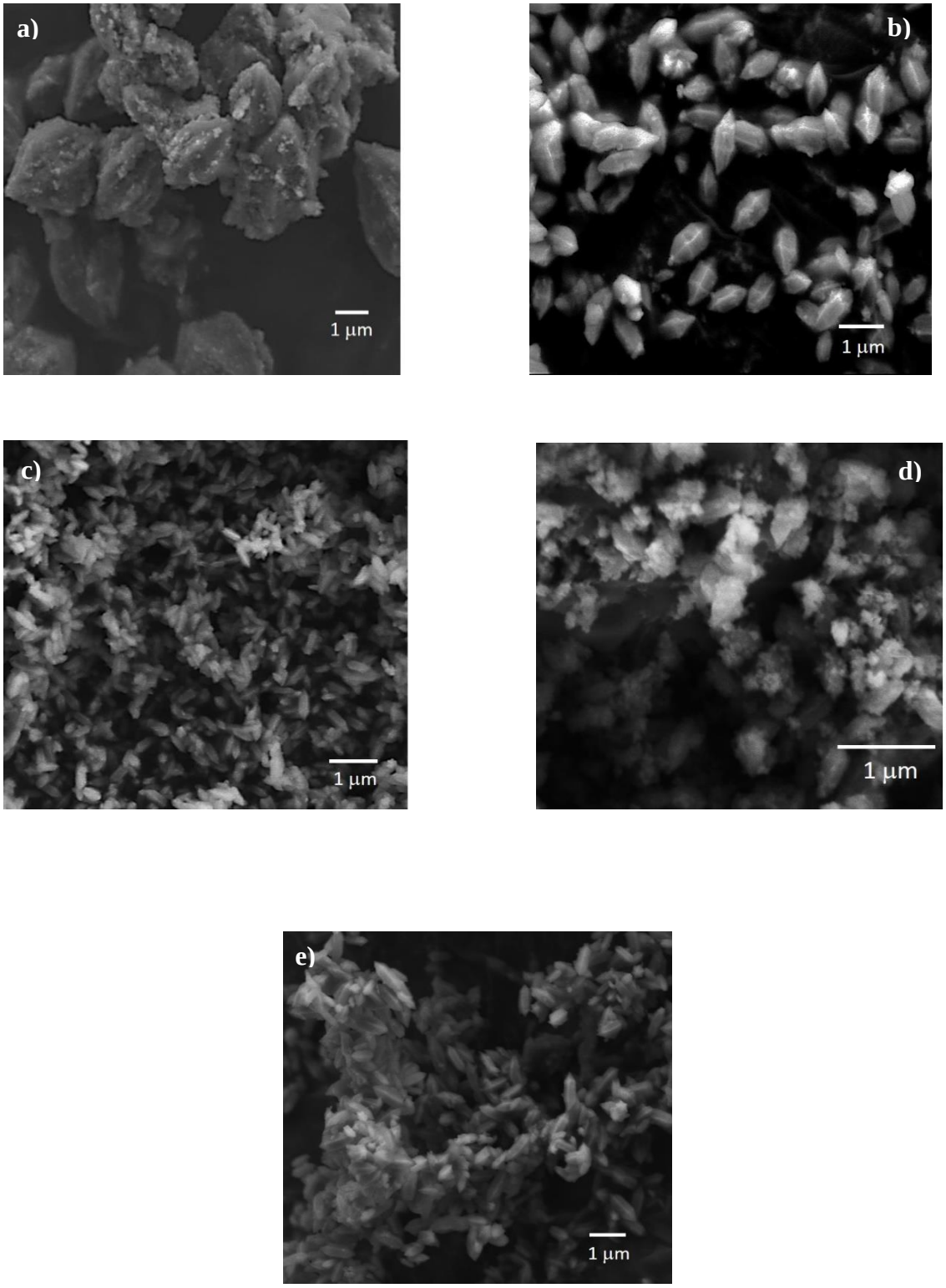

Figure 2. Scanning Electron Micrographs of MIL-88A samples (a: *Fe-fum-B2*, b: *Fe-fum-B1*, c: *Fe-fum-PP10*, d: *Fe-fum-PP5*, e: *Fe-fum-CP10*).

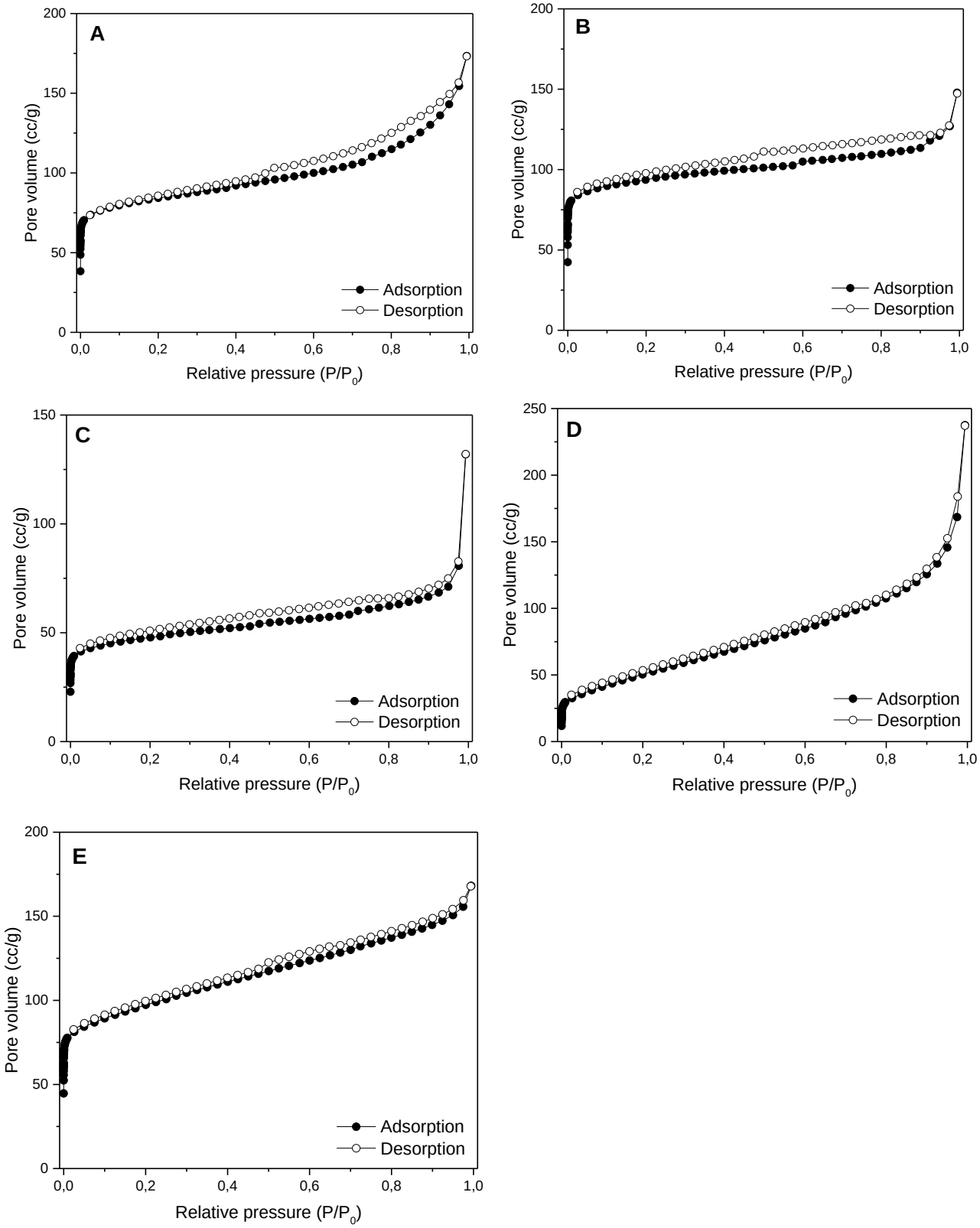

Figure 3. N_2 isotherms adsorption curves for MIL-88A samples (a: *Fe-fum-B2*, b: *Fe-fum-B1*, c: *Fe-fum-PP10*, d: *Fe-fum-PP5*, e: *Fe-fum-CP10*).

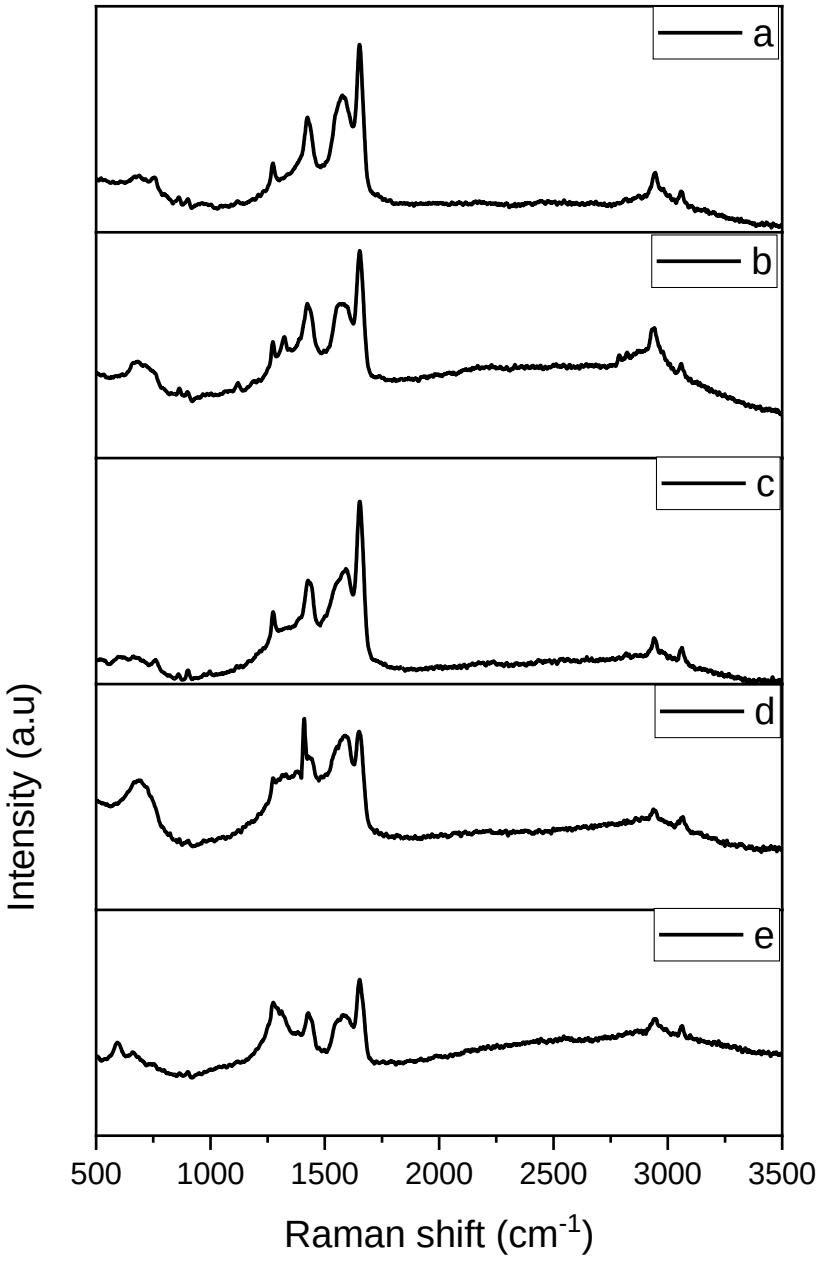

Figure 4. Raman spectra of MIL-88A samples recorded with a green light laser (λ0 = 532 nm). (a: *Fe-fum-B2*, b: *Fe-fum-B1*, c: *Fe-fum-PP10*, d: *Fe-fum-PP5*, e: *Fe-fum-CP10*).

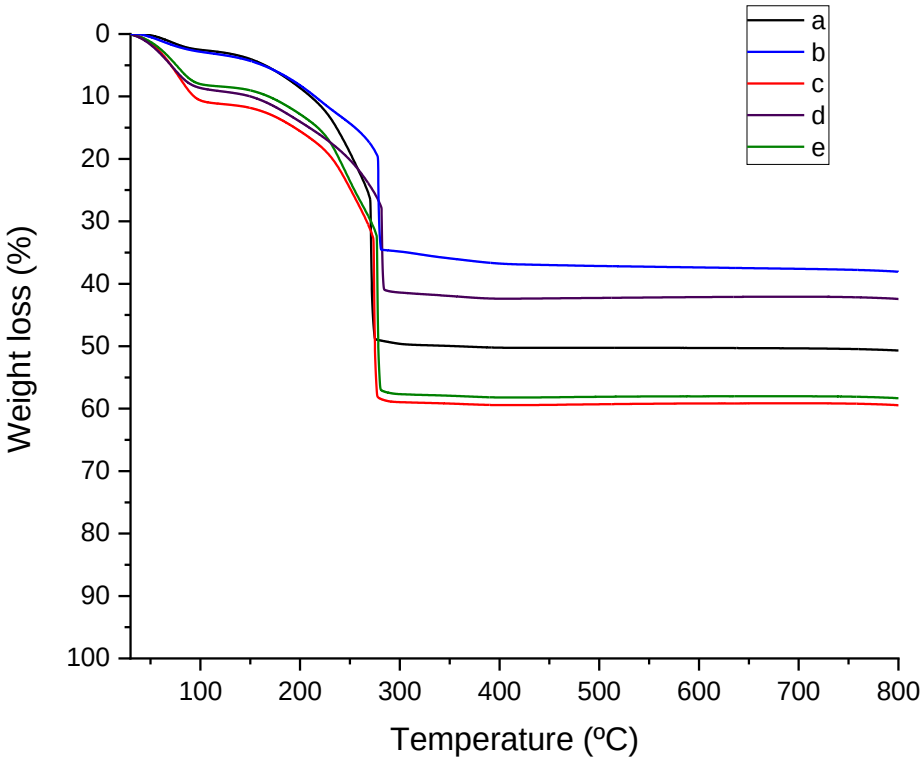

Figure 5. Thermogravimetric Analysis curves for MIL-88A samples. (a: *Fe-fum-B2*, b: *Fe-fum-B1*, c: *Fe-fum-PP10*, d: *Fe-fum-PP5*, e: *Fe-fum-CP10*).

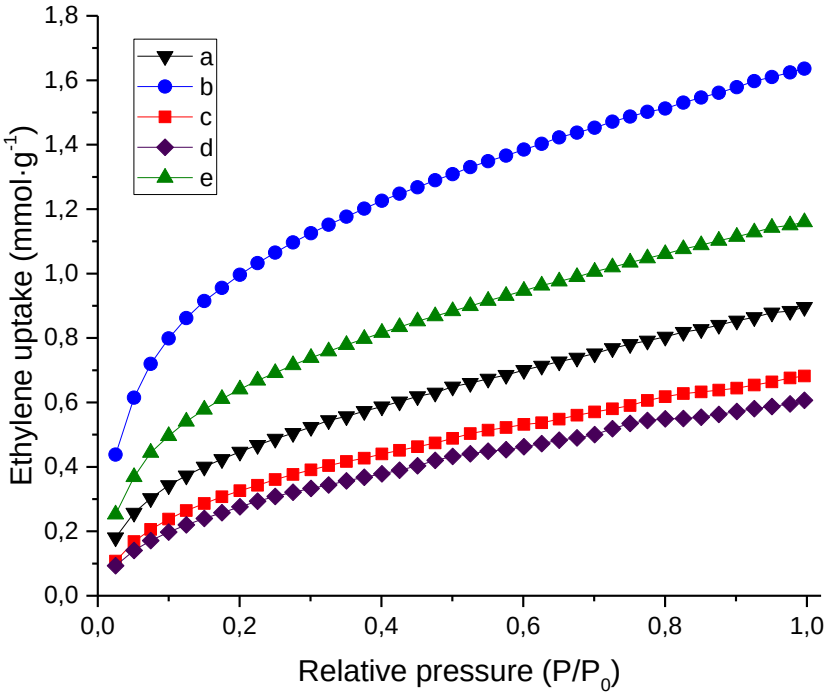

Figure 6. Ethylene adsorption curves for different MIL88-A (a: *Fe-fum-B2*, b: *Fe-fum-B1*, c: *Fe-fum-PP10*, d: *Fe-fum-PP5*, e: *Fe-fum-CP10*).

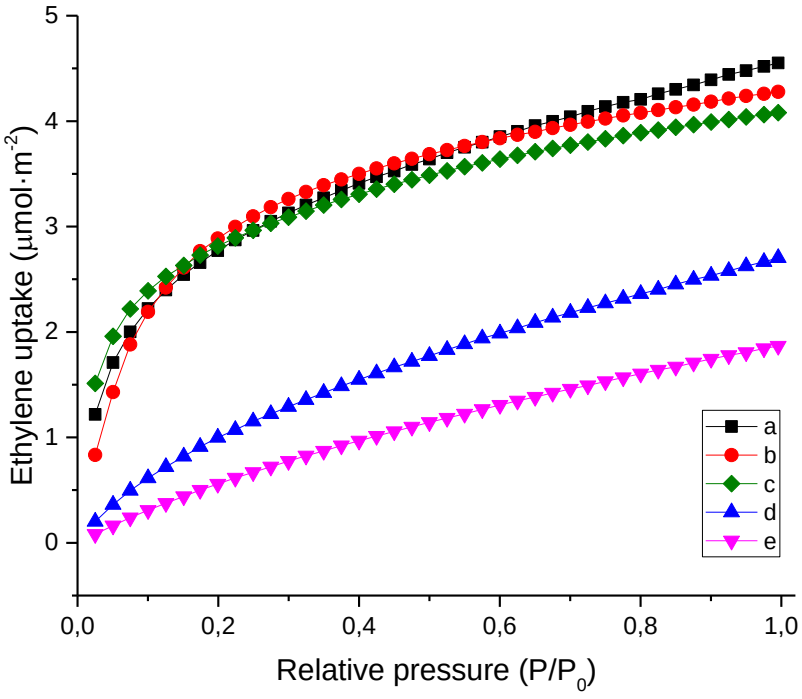

Figure 7. Ethylene adsorption curves for different MOF materials (a: *Fe-fum-B1*, b: *A520-BASF*, c: *HKUST-1*, d: *MOF-801*, e: *UiO-66*).

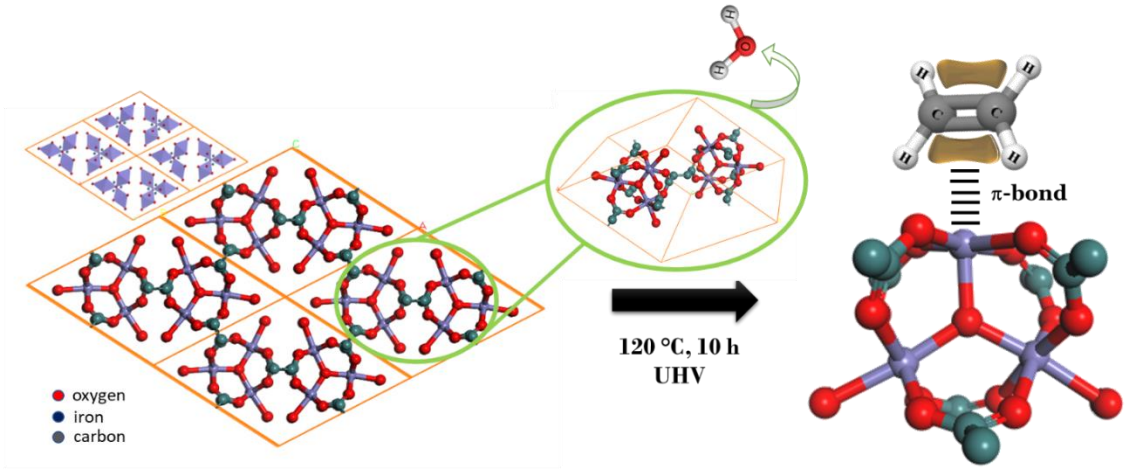

Figure 8. Mechanism of adsorption of ethylene on MIL-88A by Fe-π interactions.

SUPPLEMENTARY INFORMATION

Fast ultrasound-assisted synthesis of highly crystalline MIL-88A particles and their application as ethylene adsorbents

Juan Amaro-Gahete,[1] Rafael Klee,[1] Dolores Esquivel,* José Rafael Ruiz, César Jiménez-Sanchidrián, Francisco José Romero-Salguero.*

Departamento de Química Orgánica, Instituto Universitario de Investigación en Química Fina y Nanoquímica IUIQFN, Facultad de Ciencias, Universidad de Córdoba, Campus de Rabanales, Edificio Marie Curie, E-14071 Córdoba, Spain.

*Corresponding authors: D. Esquivel (e-mail: q12esmem@uco.es, tel.: 957211050); F. J. Romero-Salguero (e-mail: qo2rosaf@uco.es, tel.: 957218638)

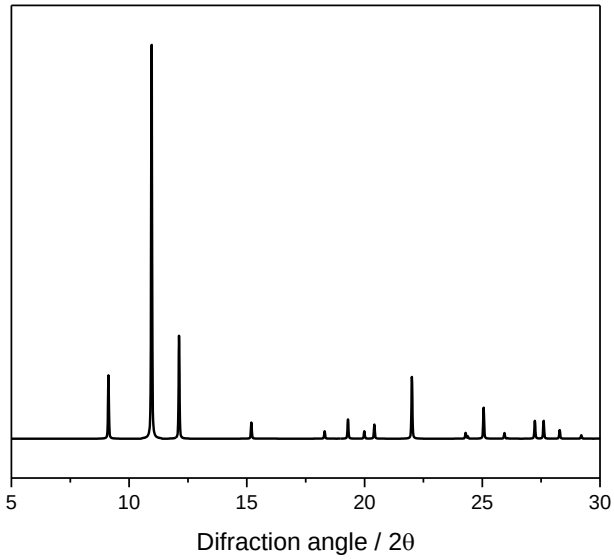

Figure S1. Simulated XRD pattern of MIL-88A

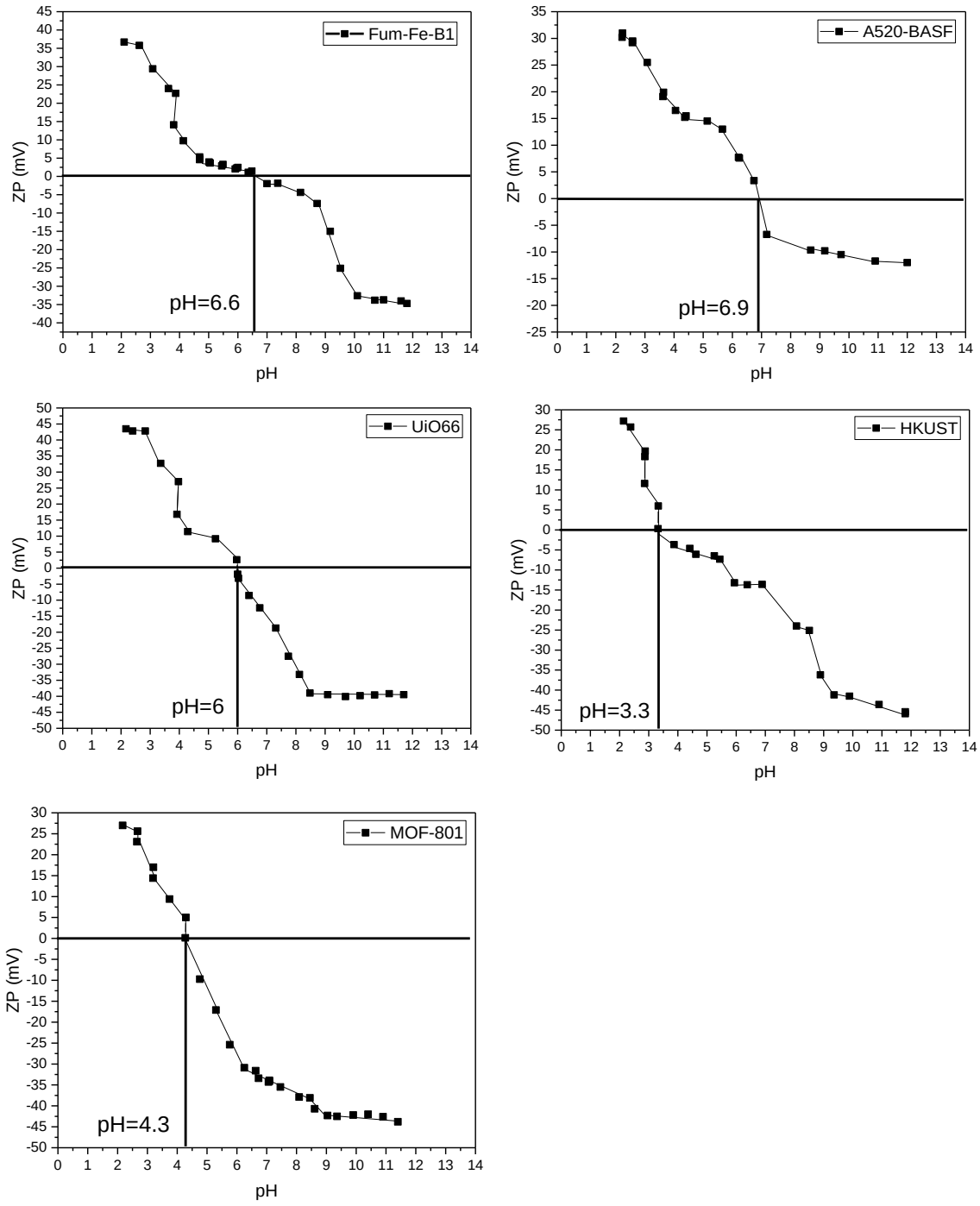

Figure S2. Variation of zeta potential as a function of pH for studied MOF materials.

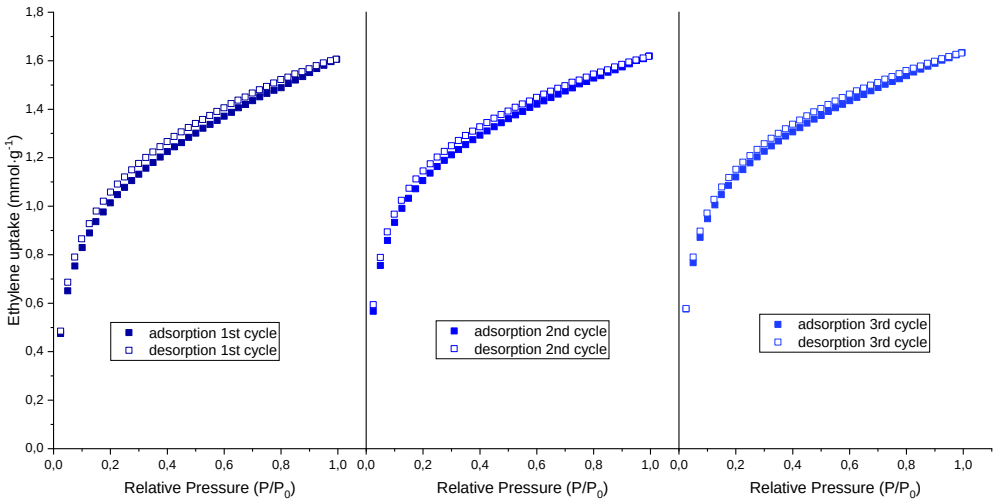

Figure S3. Consecutive ethylene adsorption-desorption cycles for Fe-fum-B1.

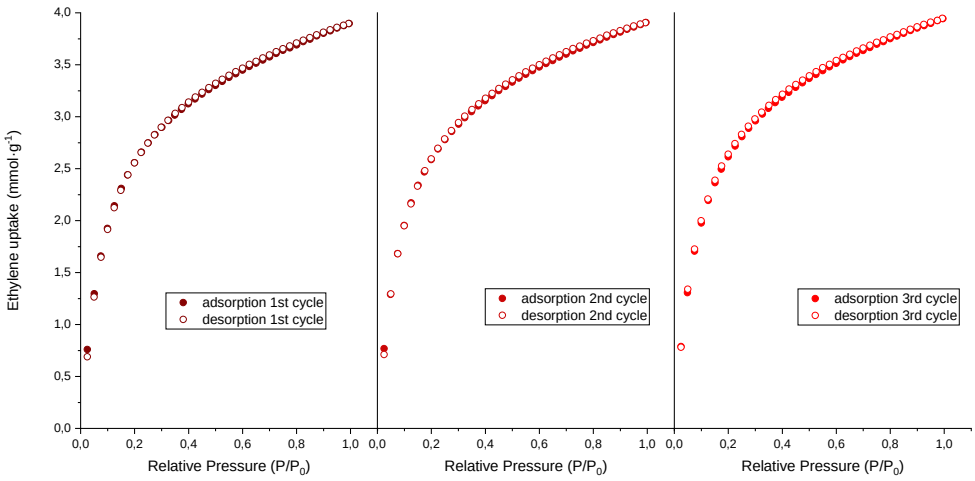

Figure S4. Consecutive ethylene adsorption-desorption cycles for A520-BASF.

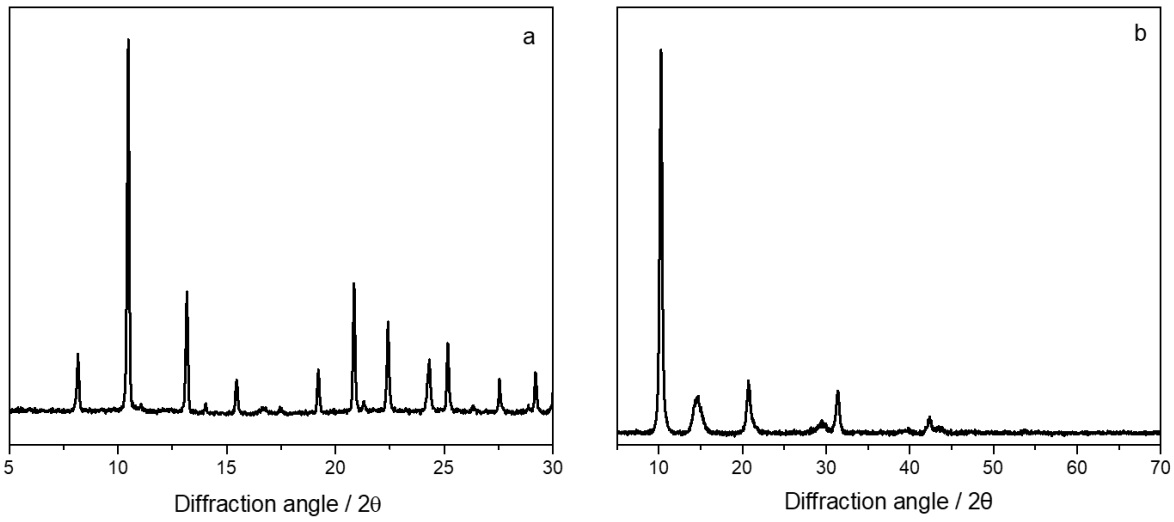

Figure S5. XRD analysis after three consecutive ethylene adsorption-desorption cycles for a) Fum-Fe-B1 and b) A520-BASF.